Available online at www.sciencedirect.com

ScienceDirect

Energy Procedia 1 (2009) 3477–3484

Energy Procedia

www.elsevier.com/locate/procedia

GHGT-9

Transport and storage of CO_2 in natural gas hydrate reservoirs

Geir Ersland*, Jarle Husebø, Arne Graue, Bjørn Kvamme

Department of Physics and Technology, University of Bergen, Allegaten 55, 5007 Bergen, Norway

Abstract

Storage of CO_2 in natural gas hydrate reservoirs may offer stable long term deposition of a greenhouse gas while benefiting from methane production, without requiring heat. By exposing hydrate to a thermodynamically preferred hydrate former, CO_2, the hydrate may be maintained macroscopically in the solid state and retain the stability of the formation. One of the concerns, however, is the flow capacity in such reservoirs. This in turn depends on three factors; 1) thermodynamic destabilization of hydrate in small pores due to capillary effects, 2) the presence of liquid channels separating the hydrate from the mineral surfaces and 3) the connectivity of gas- or liquid filled pores and channels. This paper reports experimental results of CH_4-CO_2 exchange within sandstone pores and measurements of gas permeability during stages of hydrate growth in sandstone core plugs. Interactions between minerals and surrounding molecules are also discussed. The formation of methane hydrate in porous media was monitored and quantified with magnetic resonance imaging techniques (MRI). Hydrate growth pattern within the porous rock is discussed along with measurements of gas permeability at various hydrate saturations. Gas permeability was measured at steady state flow of methane through the hydrate-bearing core sample. Experiments on CO_2 injection in hydrate-bearing sediments was conducted in a similar fashion. By use of MRI and an experimental system designed for precise and stabile pressure and temperature controls flow of methane and CO_2 through the sandstone core proved to be possible for hydrate saturations exceeding 60 %.

Keywords: CO_2-CH_4 exchange; MRI; permeability

1. Introduction

Storage of CO_2 in natural gas hydrate reservoirs may offer stable long-term storage of a greenhouse gas while benefiting from methane production, without requiring heat [1-5]. Up to date there is only very limited *in situ* information on real reservoirs producing natural gas from hydrate fields. The published data on these reservoirs are very limited, however, it is known that large quantities of natural gas is trapped beneath permafrost in the arctic regions. Some of these hydrate reservoirs are mainly trapped by the permafrost itself and could be released in the

* Corresponding author. Tel.: +47 55582868; fax: +47 55 58 94 40.
E-mail address: geir.ersland@ift.uib.no.

doi:10.1016/j.egypro.2009.02.139

near future as the permafrost regions diminishes. Controlled exploitation of these reservoirs would therefore be a win-win situation. Laboratory experiments, theoretical modelling and reservoir simulations may help establish the necessary insights into the physics that govern the stability and dynamics of gas hydrates in nature.. This study is part of an ongoing effort to help determine if gas hydrates may become a viable energy target for the future. In particular, we examine the possibilities for carbon dioxide injection in hydrate reservoirs as an approach for exploitation through exchange between the in situ natural gas and injected CO_2.

The strategy of storing a climate-altering gas while simultaneously benefiting from natural gas recovery may represent an attractive future option for several reasons: (1) The risks associated with climate change demand large-scale initiatives aimed at reduced emission of CO_2. Considerable recent attention has been paid to CO_2 storage in geological reservoirs as one way of dealing with global warming. Hydrate reservoirs represent a huge sequestration potential given the intrinsic properties of gas hydrates. (2) Carbon dioxide hydrates are thermodynamically more stable than natural gas hydrates. Dissociation of hydrate resulting in leakage of a green house gas to the atmosphere would therefore be more likely and more severe for methane hydrates (~25 times). (3) The apparent absence of large-scale melting of hydrates during the CO_2-CH_4- exchange may have significant implications for commercial aspects of this exploitation strategy.

The process of solid state exchange is possible due to free energy differences, but the mechanisms of hydrate reformation are not yet fully understood. Yoon et al. [6] and Ota et al. [7] studied the reformation process in a high pressure cell using powdered CH_4 hydrate as a starting material and then replacing methane gas in the cell with CO_2. They observed a fairly rapid initial conversion during the first 200 minutes, which then slowed down significantly. An inherent limitation in this experiment is the absence of mineral surfaces and the corresponding impact of liquid like structures separating typical sandstone minerals from hydrate. These liquid channels will result in transport channels as well as increased hydrate/fluid contact areas. The sweep efficiency both at pore scale and reservoir scale will thus be a decisive parameter for injection, CO_2 storage and CH_4 production. The objective of this study was to examine the possibilities for carbon dioxide injection in gas-water-hydrate systems at realistic conditions, and to obtain permeability data needed for numerical models at different levels.

2. Technique and procedures

The experimental system consists of the sandstone core sample, a core holder to maintain the sample at high pressure and low temperature, a high pressure control system (overburden), inlet and outlet pumps, a differential pressure transducer and the MRI to monitor the distribution of water, hydrate and methane (Figure 1). The MRI measures hydrate as the loss of intensity when the liquid water converts to solid hydrate. The porous rock samples used are Bentheim sandstone core plugs, with 22-23 % porosity and absolute (water) permeability of 1.1 Darcy. The sandstone exhibited uniform pore geometry with an average pore diameter of 125 microns

Fluorinert (FC-84) was used as both the confining fluid and the temperature control fluid. Fluorinert is a fluorocarbon and contains no hydrogen atoms, thus it is not imaged by MRI, and its low dielectric properties minimize RF losses. This fluid was maintained at the desired pressure while circulated through the cooling system and cell by the recirculation pump (Figure 1). The strong magnetic field associated with MRI required that all temperature- and pump controllers were positioned several meters away from the magnet. The high-pressure coolant lines were centered inside a low pressure PVC jacket with its own temperature-controlled circulating fluid to maximize heat exchange prior to the Fluorinert enters the MRI cell. This feature made the temperature control accurate to ± 0.1 C during weeks of operation.

Two core plug geometries were used in these experiments: The first arrangement, used for the CO2-CH4 – exchange experiments split an original cylinder down the long axis of the plug and inserted a 4 mm thick polyoxymethylene, POM, spacer between the two halves. The second was a standard cylindrical plug, 3.75 cm diameter and varying lengths between 6 and 10 cm, the second arrangement with an open fracture down the long axis of the plug. The supporting frame so that fluids could easily enter and leave the spacer. The purpose of the spacer was to simulate a fracture opening in the sample where fluids had enhanced access to the porous media. This fracture increased the surface area for exposing 1) methane to the plug during the hydrate formation stage and 2) liquid carbon dioxide during the methane replacement stage. These experiments were prepared as follows: The high-pressure cell was installed, lines connected and a vacuum applied to the pore space of the core and spacer that was subsequently filled with methane gas. After the methane was brought to 1200 psig, with the confining pressure concurrently increased to ca.1700 psig, a pre-determined amount of water was pumped in to the fracture and

imbibed into the two core-halves to produce an initial water saturation of about 45% PV. A more detailed description of the core arrangement and results from similar experiments are previously published in Graue et al. [1]. The water was imaged to determine both the quantitative amount and distribution. The water-wet sandstone core imbibed the water, rapidly producing a fairly uniform vertical and horizontal distribution throughout the core.

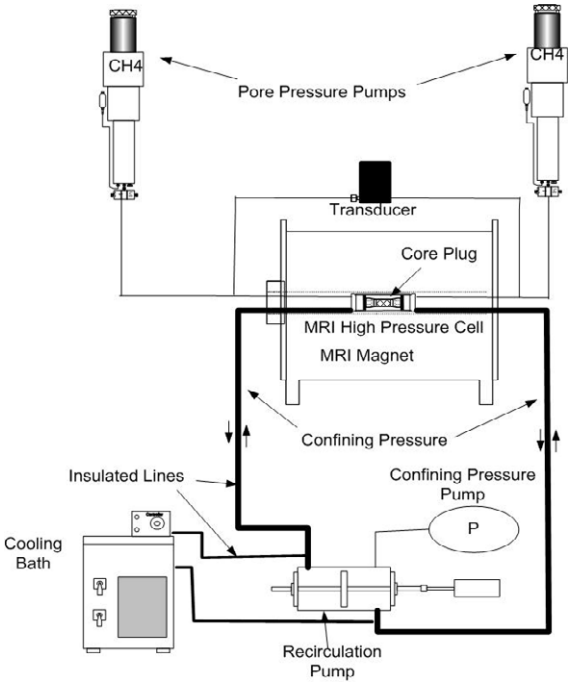

Figure 1 Overall system

Two different methods were used to establish uniform water saturations in the partially saturated whole core sample that was used for CO_2-injection experiments and when measuring gas permeability in during stages of hydrate growth. The first approach started with a fully water-saturated core assembled in the core holder. Uniform saturation distributions were established by pulling vacuum from one end. Average MRI intensity was used to plot the saturation as function of time during desaturation. The evacuation valve was closed and methane was introduced to the system when reaching the predefined water saturation. The idea behind this approach was to establish uniform saturations of methane and water without introducing air. The saturation was established outside the cell in later experiments. This way the flow lines were kept dry. When assembled, several pore volumes of methane were injected through the core to minimize the amount of air in the system. Hydrate formed without problems for both methods, with no distinct difference in induction time or formation rate, but the latter method eliminated hydrate formation in the lines.

3. Methane production by CO_2-replacement

The artificial fracture established along the cylindrical axis of the plug of known volume and orientation provided greater control for introducing gases and/or liquids into the sandstone sample. The fracture frame was used to introduce methane during the initial hydrate formation, expose carbon dioxide to methane hydrate in the porous media and collect the methane expelled from the core plug during the carbon dioxide soak at 1200 psi.

When the hydrate formation ceased (low MRI signal in core) the spacer and connected lines were flushed at constant pressure (1200 psig) with liquid CO_2. Figure 2 shows a series of MRI images collected from the core with spacer after CO_2 was injected to remove methane from the spacer. At this time the MRI images revealed very low signal, due to hydrates occupying the major part of the pore space, and CO_2 was occupying the fracture volume. CO_2 contains no hydrogen and was therefore not imaged. At this time the system was then closed and CO_2 was

allowed to diffuse into the two core halves and methane was allowed to be produced back into the spacer. The second image (B) was acquired 112 hours after the flush, at which time the MRI signal reappears in the fracture. C-D show successive images, obtained after 181 and 604 hours respectively, as methane continuously was produced into the spacer.

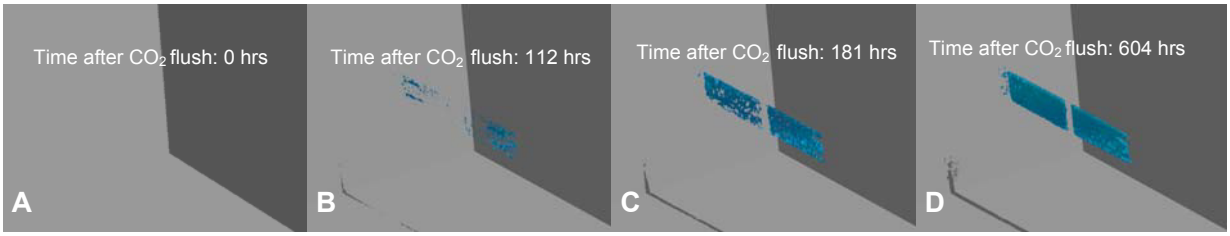

Figure 2 Methane production from gas hydrates into the open fracture

Diffusion processes appeared to be the dominant driving mechanism in supplying CO_2 to the methane hydrate reaction sites and the concomitant increase of methane in the fracture. The exchange continued over several weeks.

Another observation is the apparent absence of large-scale melting of hydrates during the CO_2-CH_4-exchange. All the experiments run in this system did not detect any significant increase in MRI signal in the hydrate saturated cores that would indicate the presence of free water during CO_2 exchange. This was verified by the evaluation of the MRI signal intensity in the core halves once CO_2 exchange began. MRI intensity remained constant or was even less than the baseline value after the completion of hydrate formation. The exchange process did not cause significant dissociation of the hydrate, at least on the scale of the MRI's spatial resolution of ~0.8 mm^3.

4. CO_2 injection in hydrate-bearing sediments

An immediate question arises if one tries to export the above results to hydrate field scale: What is the flow capacity of gas hydrate accumulation? It is obvious that the area of contact between hydrate and CO_2 as well as available transport channels play key roles in the exchange process. The sweep efficiency both at pore scale and reservoir scale will thus be a decisive parameter for injection, CO_2 storage and CH_4 production. The next step in this project was therefore to examine the possibilities for carbon dioxide injection in gas-water-hydrate systems, and to obtain permeability data for numerical models at different levels. Permeability will vary over a wide range, depending on the properties of the sediment, the hydrate saturation of and growth patterns of gas hydrate. Field scale information of *in situ* permeability of hydrate bearing sediments is very limited, and laboratory studies of permeability is needed as input to numerical simulations of production predictions in all production schemes based on both mass transfer and hydrate dissociation induced by pressure depletion.

The gas hydrate formation starts spontaneously as the temperature move towards gas hydrate equilibrium conditions and was detected as a sudden consumption of methane and a corresponding drop in MRI intensity in the core (Figure 3). The system temperature was never allowed below 3.6 $^{\circ}C$ to ensure only three phases were present at any time (methane gas, liquid water and solid methane hydrate). The brine used was deionized water with 0.1 wt% NaCl added.

This test first objective was to see if CO_2 could be injected through a whole core sample with hydrates filling ~60 % of the pore space. Figure 3 shows The MRI signal response in the core during hydrate formation. The rate of hydrate formation declined after an initial rapid growth of 16 hours, but continued for over one week. The core sample was extended by a 1 mm Teflon spacer at both the inlet and outlet face of the core. This was done to provide bulk MRI signal at both ends, where fluids were injected and produced. CO_2 was injected after ca. 250 hours after almost complete hydrate formation. The MRI signal in the core drops somewhat when CO_2 was injected in the core and displaced free methane in the pore space. The MRI signal in both inlet and outlet spacers drops after CO_2 was introduced which suggest an almost immediate breakthrough.

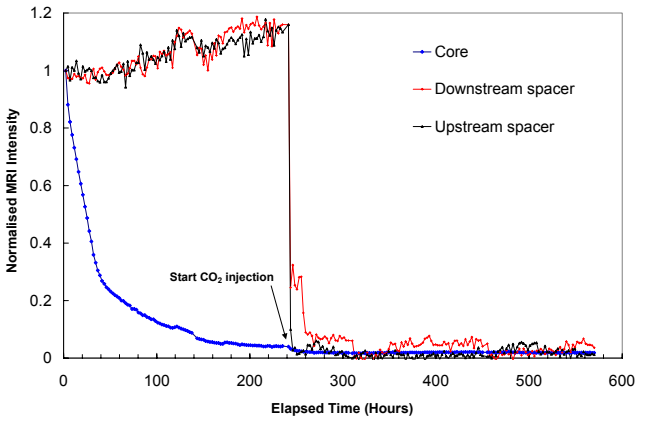

Figure 3 MRI intensity

5. Measurements of gas permeability in gas-water-hydrate systems

MRI images of hydrate formation are shown in Figure 3 for a whole core with 50 % initial brine and 50 % methane saturation. The first image was acquired before cooling with water as the predominant signal source. Images 2-4 in Figure 3 show uniform growth throughout the core as expected for an evenly distributed and well connected gas phase.

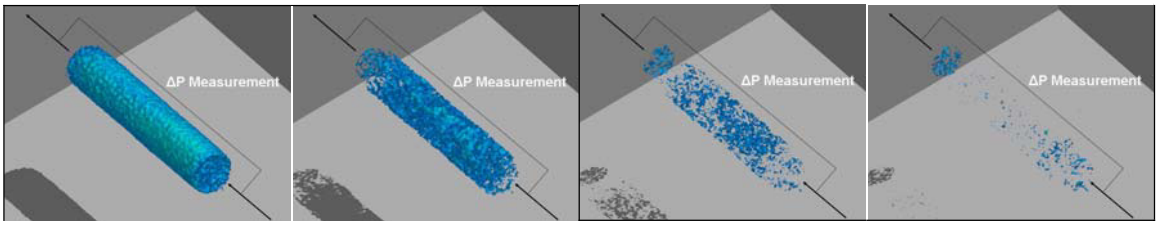

Figure 4 Hydrate formation (0, 23, 30, 36 hrs)

Very little free water was left behind (< 3%), however, for higher salinities (3-5 wt% NaCl), more of the water was not converted. The permeability measurements were acquired at stages of hydrate growth as indicated in the 3D MRI images in Figure 4. However, due to rapid initial growth, fast MRI profiling was used to determine saturations and ensure no change in saturation before and after each permeability measurement.

Six experiments were conducted to measure gas permeability in hydrate saturated pores. Table one list crude values of gas permeability before and after hydrate formation along with saturations of gas, water and hydrate. Measurements are performed with the same flow rate for individual experiments are not corrected for inertial flow resistance and should not be regarded as absolute values.

Figure 5 Evolution of gas permeability during hydrate growth for initial water saturation of 48% (left) and gas permeability before and after hydrate formation for six individual experiments (right)

For the lower initial water saturations (exp. 1&2) the permeability drops notably more for experiment 1 where more of the water is converted to hydrate. The later four experiments with initial saturations between 47 and 51 percent are relatively consistent and characterized with a permeability drop between one and two orders of magnitude. These results are in agreement with recent work on gas permeability measured in sand samples [11]. The most obvious result is that gas permeability drops with increased formation of gas hydrates. Hydrates will expand and act as an extension of the solid grain space resulting in pore-filling reduction of porosity. Calculations show that a given amount of water occupies 26 percent more of the pore space when converted from liquid water to methane hydrate.

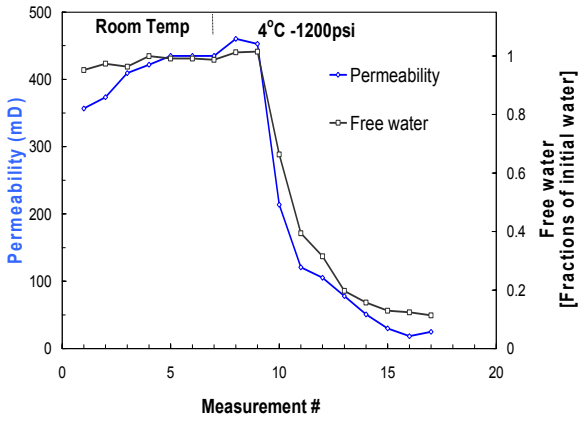

Exp #	$S_w/S_g/S_h$	k_{app}(mD)
1	33/67/0	670
	2/57/41	143
2	34/66/0	410
	11/60/29	217
3	47/53/0	356
	11/44/45	25
4	48/52/0	157
	3/41/56	13
5	51/49/0	115
	4/36/60	4
6	36/64/0	248
	2/40/58	7

Figure 5 Gas permeability at stages of hydrate growth

Figure 5 shows a typical evolution of gas permeability as function of hydrate growth. Clearly, the resistance to flow, which depends on hydrate micro geometry and growth pattern, will increase as the hydrate saturation increases and eventually occupies a portion of the pore space large enough to render the core impermeable. Fundamental questions that arise are: What is the critical gas saturation in gas-water-hydrate systems (lowest S_g where $k_g > 0$)? What growth pattern is present in these experiments and how does the experiment mimic hydrate accumulations in nature?

Figure 6 summarize all permeability measurement plotted as function of hydrate saturation and gas saturation. For high hydrate saturations and low water saturation (below 4 %) the apparent gas permeability is reduced to a few mD. Figure 6 (left) shows gas permeability as function of the open gas volume in the core. The agreement between experiments is good and extrapolation suggests critical gas saturation around 35 %. Non-porous hydrates work as a barrier to gas flow since they are not likely to move under moderate pressure gradients. By contrast, gas can more easily penetrate through a mobile water phase; the flow paths become more tortuous, which suggest higher critical gas saturations for hydrate-saturated pores compared to pure water-gas systems.

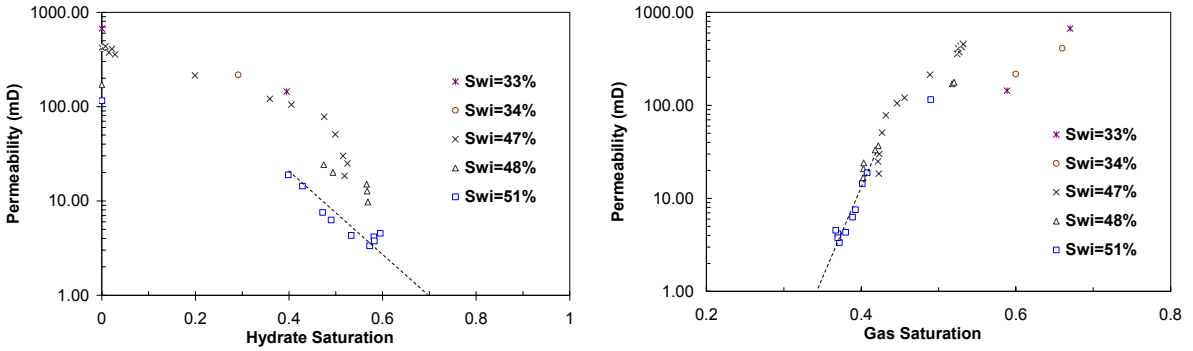

Figure 6 Gas permeability vs. hydrate saturation (right) and gas saturation (left)

In reservoirs with gas hydrate accumulations it is recognized that there is an important interaction between the growth pattern of hydrate in the porous sediment, and the resulting hydraulic permeability of the formation [12]. Helgerud [13] proposed four scenarios for hydrate growth in porous media: (a) Hydrate forms preferentially at grain contacts, acting as cement even in small quantities. (b) Hydrate coats grains more or less uniformly, progressively cementing them as the hydrate volume increases. (c) Hydrate grows in the interior of pores partially supporting the frame. (d) Hydrate grows without significant interaction with the frame. The capillary effects on hydrate stability can be incorporated through the incorporations of interface free energy in the classical adsorption theories [3].

Experiments on hydrate formation in small silica pores [14] indicate that the effects are limited to pores of sizes smaller than ~30 Å, but may vary for other minerals and other conditions. Relative to the classification of Helgerud there is theoretical and experimental evidence that hydrate may stick to clay surfaces [15, 16]. Preferential water structure at calcite surfaces prevents hydrate from sticking to these types of mineral surfaces [17].

Kleinberg et al. [18] interpreted NMR T_2-distributions to suggest that hydrates, when formed from free gas, occupy the largest pores in consolidated rock. He argued that it is only there that both reactants are present in substantial quantities; gaseous methane, a non-wetting phase, will be confined to the largest diameter pore spaces. Kleinberg's experiments were carried out with methane as the limiting component for hydrate formation. Water was introduced in a core previously saturated with methane gas. In the present experiment, however, with water being the limiting hydrate forming component, the growth pattern was somewhat different. In either case, due to the low solubility of methane in water, hydrates preferentially start forming at the gas-water interface [19]. In the case of Kleinberg, the gas bubbles gradually were consumed in place, leaving hydrates surrounded by water as nodules were centered in the pore. In our case, it can be argued that hydrates start forming at the gas-water interface, grow towards the pore wall and expand towards the center. This may be a model for downward movement of the Gas Hydrate Stability Zone (GHSZ) through a gas reservoir. This may occur as a result of change in the geothermal profile, and may be a mechanism for particularly high hydrate saturations [18]. With respect to free water this growth pattern reveals several possible outcomes: (a) The hydrate grows until it finally coats the mineral surface, leaving an insignificant amount of water in the liquid state. (b) A film of water is wetting the mineral surface. (c) A film of water is wetting the mineral surface and/or there are liquid channels between hydrate crystals. Tohidi et al. [20] studied tetrahydrofuran hydrate formed from a miscible solution, methane hydrate formed from free gas in water, and carbon dioxide hydrate formed from dissolved gas in water. In all experiments formation of hydrate left a thin layer of liquid water wetting the solid surfaces. Well log data shows that sediment grains remain liquid-water wet in both arctic and marine sediments, which are consistent with earlier permafrost results [21-22]. High salinity is known to restrict hydrate formation [23-24] which suggest that the water film thickness is likely to be dependent on the salinity of the formation brine. High salt concentration may even leave pools of supersaturated water as salt is increasingly concentrated in the remaining water when more of the water is crystallized to hydrate.

6. Conclusions

MRI imaging was successfully used to map and quantify hydrate saturation and CH_4-CO_2 exchange in sandstone core plugs. CO_2 injection in core plugs with high hydrate saturation (~ 60 %) was performed. Gas permeability was measured during hydrate growth in six experiments with initial water saturations ranging from 33–52 per cent. Initial water saturation and the corresponding hydrate saturation after hydrate formation had major impact on the gas permeability. As expected, gas permeability decreased rapidly as hydrate formed. For hydrate saturation ~ 60 %, the apparent gas permeability was reduced to a few mD in a 1.1 Darcy core. Hydrate growth pattern affects the relative permeability curves for water-gas-hydrate systems. Factors controlling the latter include mineralogy and texture, water salinity, gas composition, and whether hydrate forms from free or dissolved gas. Our results are relevant to situations in which water is exposed to free methane.

7. Acknowledgements

The authors acknowledge the contributions from Jim Stevens, James J. Howard at ConocoPhillips and Bernie A. Baldwin, Green Country Petrophysics LLC in obtaining the experimental MRI results.

8. References

[1] A. Graue, B. Kvamme, B.A. Baldwin, J. Stevens, J. Howard, E. Aspenes, G. Ersland, J. Husebø and D. Zornes, "MRI Visualization of Spontaneous Methane Production From Hydrates in Sandstone Core Plugs When Exposed to CO_2" SPE Journal (SPE 118851), Volume 13, No. 2, June 2008.

[2] Kvamme B, Graue A, Kuznetsova T, Buanes T, Ersland G. *Exploitation of natural gas hydrate reservoirs combined with long term storage of CO2*", WSEAS TRANSACTIONS on Environment and Development 2006; 2(6), 699 – 710.
[3] Kvamme B, Tanaka H. *Thermodynamic stability of hydrates for ethylene, ethane and carbon dioxide*". J.Phys.Chem. 1995; 99, 7114.
[4] Svandal A, Kuznetsova T, Kvamme B. *Thermodynamic properties interfacial structures and phase transitions in the $H_2O/CO_2/CH_4$ system*", Fluid Phase Equilibria 2006; 246, 177–184.
[5] Svandal A, Kuznetsova T, Kvamme B. *Thermodynamic properties and phase transitions in the $H_2O/CO_2/CH_4$ system*, Physical Chemistry Chemical Physics 2006; 8, 1707 - 1713.
[6] Yoon J-H, Kawamura T, Yamamoto Y, Komai T. *Transformation of Methane Hydrate to Carbon Dioxide Hydrate: In Situ Raman Spectroscopic Observations*. J. Phys. Chem. A, 2004; 108, 5057-5059.
[7] Masaki O, Abe Y, Watanabe M, Smith R L, Inomata H. *Methane recovery from methane hydrate using pressurized CO2*. Fluid Phase Equilibria, 2005, 228-229, 553-559.
[11] Seol Y, Kneafsey T, Tomutsa L, Moridis G. J. *Preliminary relative permeability estimates of methane hydrate-bearing sand. Proceedings, TOUGH 2006, Lawrence Berkeley National Laboratory, Berkeley, California, May 15-17, 2006*.
[12] Nimlett J, Ruppel C, *Permeability evolution during the formation of gas hydrates in marine sediments* J. Geophys. 2003 Res., 108(B9), 2420, doi:10.1029/2001JB001650
[13] Helgerud M.B, *Wave speeds in gas hydrates and sediments containing gas hydrates: A laboratory and modeling study*, Ph. D. Dissertation, Stanford University, 2001.
[14] Titiloye J. O, Skipper, Neal T, *Monte Carlo and molecular dynamics simulations of methane in potassium montmorillonite clay hydrates at elevated pressures and Temperatures*, Journal of Colloid and Interface Science, 2005; 282. 422–427
[15] Hwang S, Blanco M, Demiralp E, Cagin T, Goddard W.A. *The MS-Q Force Field for Clay Minerals: Application to Oil Production*. J. Phys. Chem. B 2001; 105, 4122-4127.
[16] Smith D.E. *Molecular Computer Simulations of the Swelling Properties and Interlayer Structure of Cesium Montmorillonite* Langmuir 1998; 14 (20), 5959-5967
[17] Kvamme, B., Kuznetsova, T., Uppstad, D., *Modeling excess surface energy in dry and wetted calcite systems*, submitted to Computational Materials Science, 2006.
[18] Kleinberg R.L, Flaum C, Griffin D.D, Brewer P.G, Malby G.E, Peltzer E.T, Yesinowski J.P. *Deap Sea NMR: Methane Hydrate Growth Habit in Porous Media and its Relationship to Hydraulic Permeability, Deposit Accumulation, and Submarine Slope Stability* submitted to Journal of Geophysical Research B, March 2003
[19] Kvamme B. *Initiation and growth of hydrate from nucleation theory.* International Journal of Offshore and Polar Engineering 2002; 12(4):256-262.
[20] Tohidi B, R. Anderson, M.B Clennell, R.W Burgass, A.B. Biderkab, *Visual observation of gas hydrate formation and dissociation in synthetic porous media by means of glass micromodels* Geology 2001; 29, 867-870.
[21] Murray D.R, Kleinberg R.L, Sinha B.K, Fukuhara M, Osawa O, Endo T, Namikawa T *Saturation, Acoustic properties, Growth Habit, and State of Stress of a Gas Hydrate Reservoir from Well Logs* Petrophysics April 2006; vol. 47, No 2 P. 129-137.
[22] Kleinberg R.L, D.D. Griffin *NMR measurement of permafrost: Unfrozen water assay, pore scale distribution of ice, and hydraulic permeability of sediments* Cold Regions Science and Technology 2005, V. 42, Issue 1, p. 63-77.
[23] Sloan ED, Koh CA. *Clathrate hydrates of natural gases, 3rd ed*. Boca Raton: CRC Press. 2008.
[24] Husebø J., Ersland G., Graue A., Kvamme B., Stevens J. The effect of brine salinity on fill fraction and formation pattern of methane hydrates in sandstone" Proceedings of the 6th International Conference on Gas Hydrates (ICGH 2008),Vancouver, British Columbia, CANADA, July 6-10, 2008.